Scuola Internazionale Superiore di Studi Avanzati - Trieste

Electrophysiological Properties and Modeling of Murine Vomeronasal Sensory Neurons in Acute Slice Preparations

Magister Philosophiae degree thesis

Candidate:

Ranken Shimazaki

Supervisor:

Prof. Anna Menini

September 16, 2005

SISSA – Via Beirut 2-4 – 34014 TRIESTE – ITALY

Electrophysiological Properties and Modeling of Murine Vomeronasal Sensory Neurons in Acute Slice Preparations

Magister Philosophiae degree thesis

Candidate:

Ranken Shimazaki

Supervisor:

Prof. Anna Menini

September 16, 2005

ISAS – International School for Advanced Studies
SISSA – Scuola Internazionale Superiore Studi Avanzati

VNO in Action - The Flehmen Response is a particular type of curling of the lips in ungulates, felids, and many other mammals, which facilitates the transfer of chemicals into the vomeronasal organ. This behavior allows animals to smell the urine of others in order to determine several factors. These factors can be the presence or absence of estrus, the physiological state of the animal, and how long ago the animal passed by.

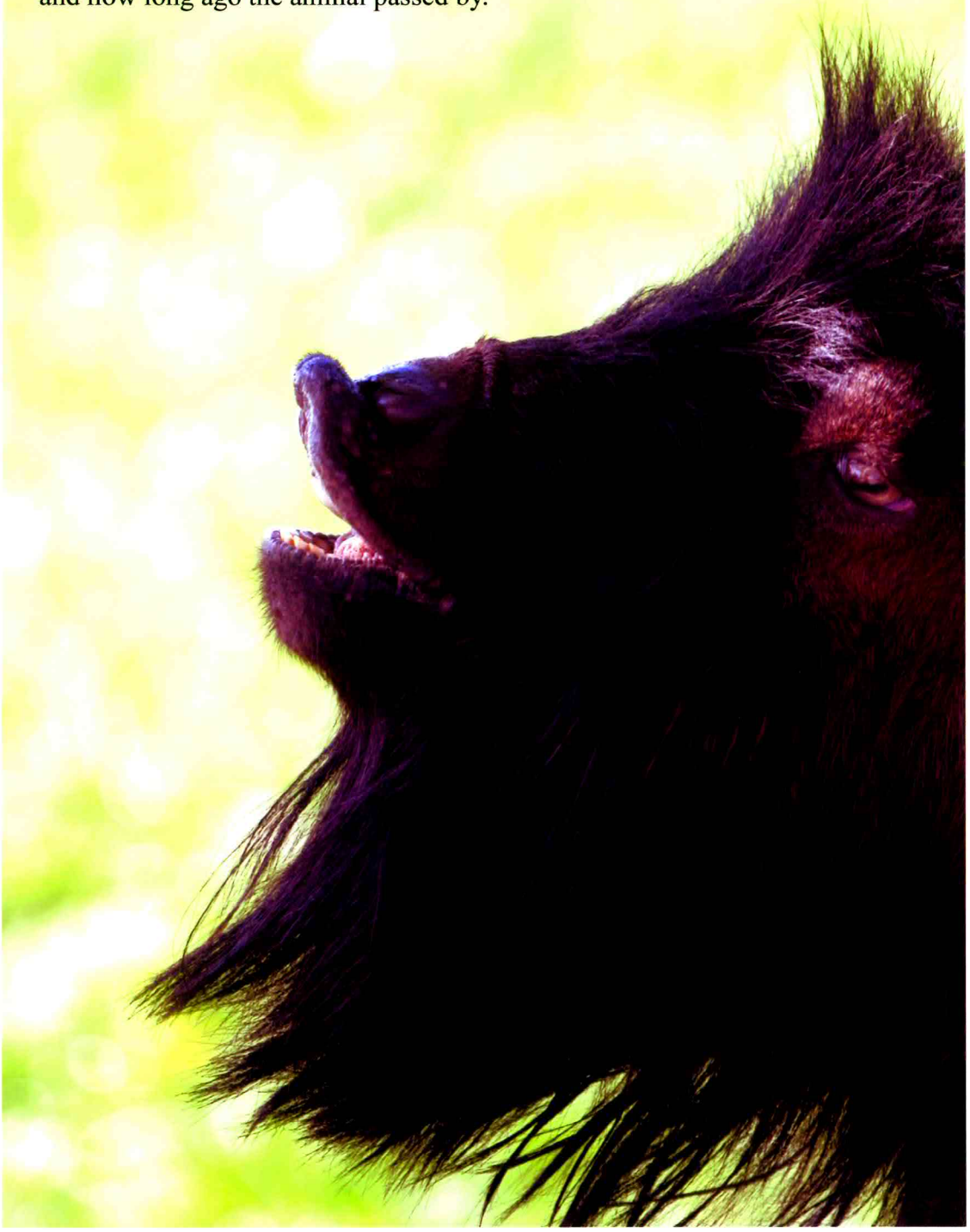

Electrophysiological Properties and Modeling of Murine Vomeronasal Sensory Neurons in Acute Slice Preparations

INTRODUCTION

Behavior may be the single most important attribute of living organisms. How behavior is controlled is therefore of obvious interest to scientists as well as the general public. The key to understanding behavior lies in the interface between the environment and the organism whose behavior and ability to survive and thrive is dependent on that environment. Pheromones provide the key link in this pathway by transferring behaviorally relevant information between members of the same species as well as between species.

Pheromones are molecules emitted by an organism, often found in sweat, urine, saliva, gland secretions, and reproductive fluids which provide information about gender, social status, sexual maturity, estrus status, and elicit behaviors such as courtship, mating, aggression, and territorial marking (**Figure 1**) (Dulac and Torello, 2003; Brennan and Keverne, 2004; Halpern and Martinez-Marcos, 2003; Holy *et al.*, 2000). Their effect can be divided into two broad categories defined by the time it takes the pheromone to elicit a given behavior in another organism. Releaser pheromones are those with a short time course, provoking a behavioral response immediately or soon after detection (i.e. aggression, mating), while pheromones acting over a longer time course are known as primer pheromones and are often mediated through the neuroendocrine system (Bigiani *et al.*, 2005; Keverne, 2000).

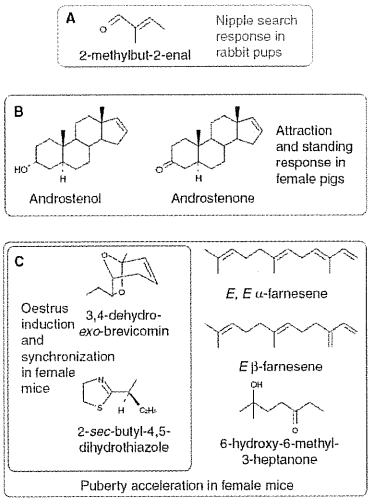

Figure 1. Mammalian pheromones and their reported behavioral effects. *A* The rabbit nipple search pheromone. *B* Androgen derivatives found in boar saliva. *C* Volatile constituents of male mouse urine specifying maleness. From Brennan and Keverne, 2004.

The importance of pheromones is evident not only by their effect on behavior, but also at the physiological level where, in most mammals, a whole organ has evolved to allow for their detection and information relay to higher cortical areas. The vomeronasal organ (VNO), also known as the organ of Jacobson, is an accessory olfactory organ located above the palate in most mammals (**Figure 2**). The VNO is encased in a protective boney and cartilaginous capsule and divided bilaterally in two by the vomer bone (**Figure 3**). Pheromones enter the VNO through the nasal cavity or through a duct connected to the oral cavities where they then enter the organ's luminal space and bind to receptors on the microvilli of vomeronasal sensory neurons (VSNs) embedded in the sensory epithelium (Doving and Trotier, 1998; Jacobson *et al.*, 1998). **Figure 4** shows a slice through the VNO where the sensory epithelium (SE), luminal space (L), nonsensory

epithelium (NE), blood vessel (BV), and approximate location of VSNs (V1R and V2R) can be seen.

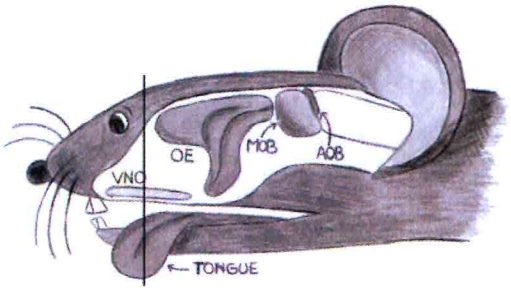

Figure 2. Illustration showing the position of the vomeronasal organ in the mouse head. *VNO* vomeronasal organ, *OE* olfactory epithelium, *MOB* main olfactory bulb, *AOB* accessory olfactory bulb. Adapted from Bigiani et al, 2005.

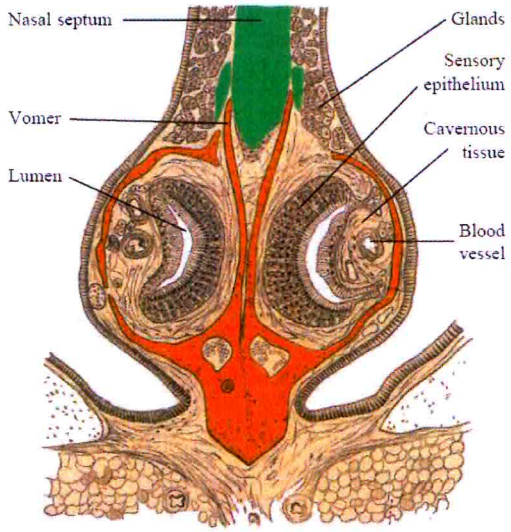

Figure 3. Cross section through the vomeronasal organ. The bilateral organization is clearly visible as well as some of the substructure inside the VNO. Pheromones enter the luminal space and bind to vomeronasal sensory neuron receptors located in the sensory epithelium. The blood vessel's pumping action facilitates pheromone exposure by constantly refreshing the luminal space. The general structure of the VNO is supported and protected by the vomer bone and cartilaginous tissue. Adapted from Doving and Trotier, 1998.

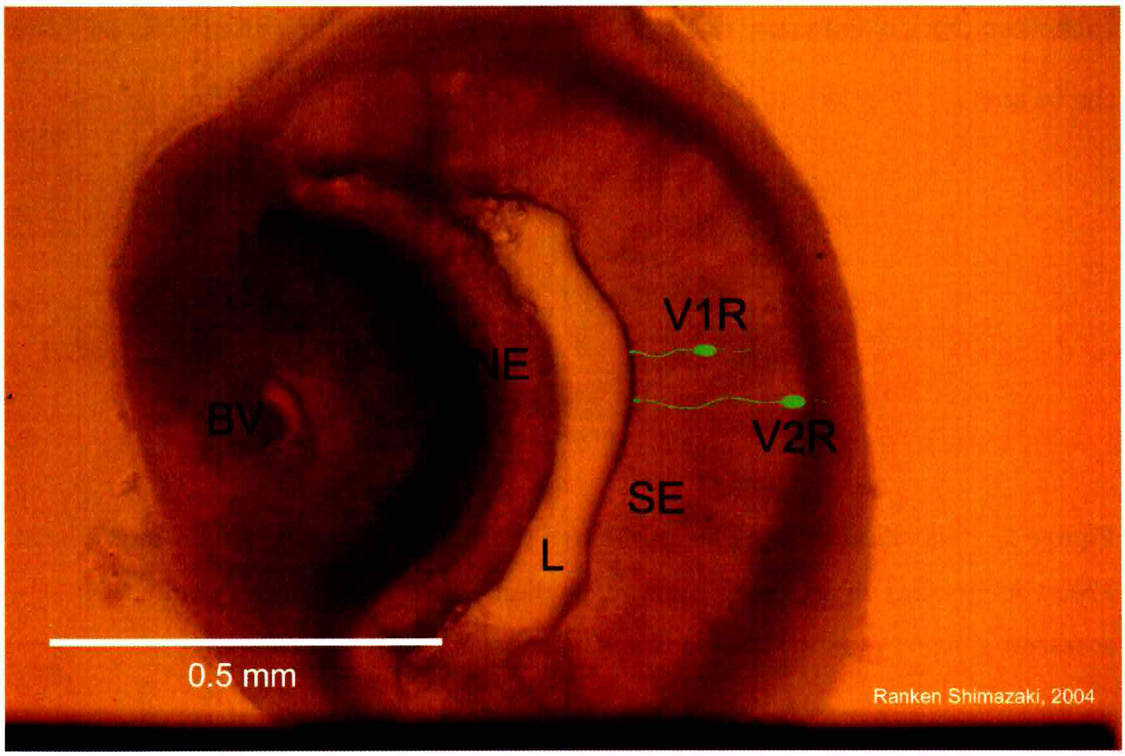

Figure 4. Cross section of the vomeronasal organ, free from the capsule and vomer bone. *BV* blood vessel, *NE* nonsensory epithelium, *L* lumen, *SE* sensory epithelium, *V1R* apical vomeronasal neuron, *V2R* basal vomeronasal neuron.

Three primary cell types exist in the sensory epithelium. Supporting cells are large, elongated, glia-like cells which serve, as the name implies, as a scaffold for other cells. Basal stem cells are also present in the sensory epithelium. The third, and functionally most important cell type is the vomeronasal sensory neuron which, like olfactory sensory neurons, are constantly being replaced from the pool of basal stem cells (Weiler *et al.*, 1999; Vaccarezza *et al.*, 1981).

VSNs are bipolar sensory cells having a cell body 10-15 μm in diameter and extending a single dendrite to the luminal surface where it enlarges into a dendritic knob with

microvilli 3-6 μm long and 0.1 μm in diameter (Ciges *et al.*, 1977) (**Figure 5**). A long axon projects from the other end of the cell body to the accessory olfactory bulb in the brain (**Figure 6**) (Brennan, 2001; Fieni *et al.*, 2003; Rodriguez *et al.*, 1999). VSNs are one of the most sensitive mammalian chemoreceptors being able to detect some chemicals, such as farnesene, at concentrations as low as 10^{-11} M (Leinders-Zufall *et al.*, 2000).

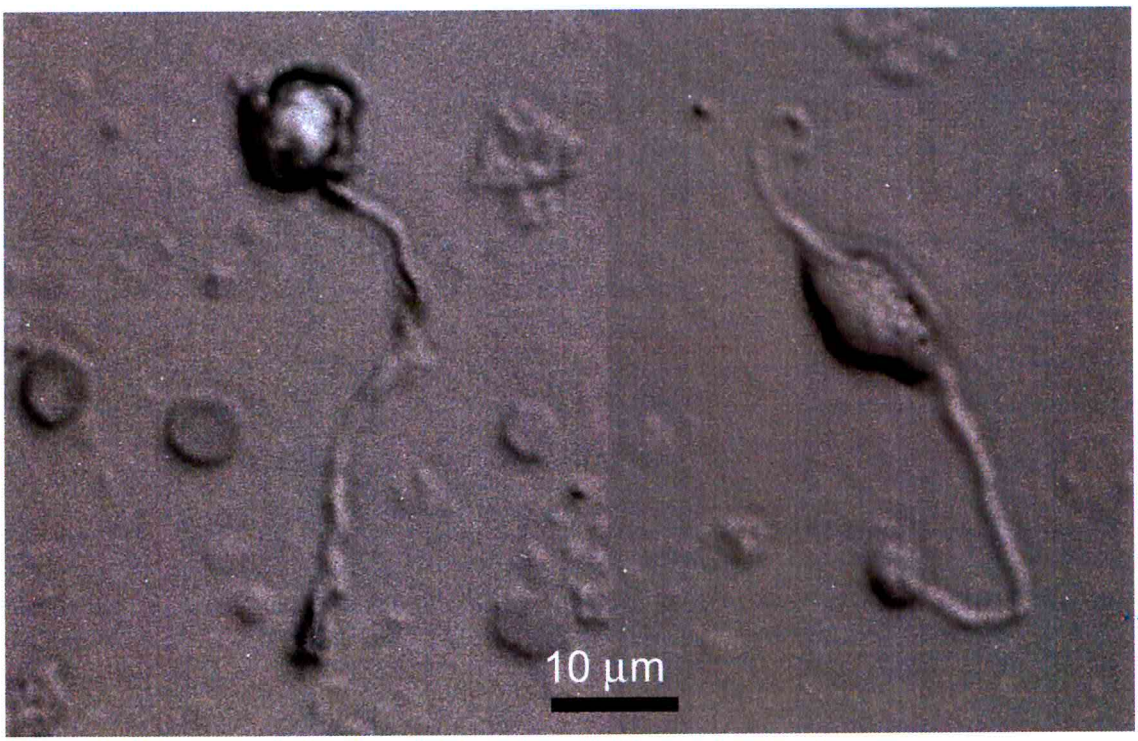

Figure 5. Dissociated vomeronasal sensory neurons. Long dendrites can be seen extending towards the bottom of the frame ending in the dendritic knob. In right-hand photo, part of the axon is also visible.

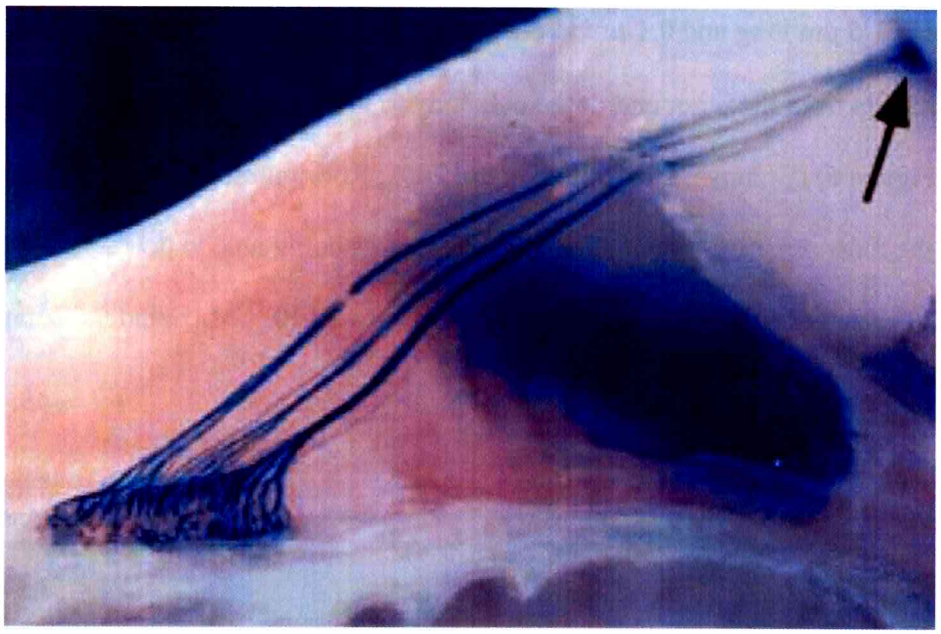

Figure 6. V2R Vomeronasal sensory neurons stained with X-gal showing axonal projections to the accessory olfactory bulb (arrow). Adapted from Rodriguez *et al.*, 1999.

Within the sensory epithelium two multigene families expressing G-protein linked receptors, V1R and V2R, have been identified, expressing ~160 and up to ~200 functional vomeronasal receptor genes, respectively (Dulac and Axel, 1995; Matsunami and Buck, 1997; Berghard and Buck, 1996; Zhang *et al.*, 2004; Herrada and Dulac, 1997; Rodriguez and Mombaerts, 2002; Ryba and Tirindelli, 1997). While sharing little similarity to main olfactory receptors, both V1R and V2Rs are seven transmembrane domain proteins and share in common the G-protein subunit $G\beta_2$ (Runnenburger *et al.*, 2002). V1Rs are associated with the G-protein subunits $G\alpha i_2$ and $G\gamma_2$, and have a short N-terminal extracellular domain. V2Rs are associated with the G-protein subunits $G\alpha o$ and $G\gamma_8$, and have a large 70 kDa extracellular N-terminal domain, similar to metabotropic glutamate receptors, both of which belong to group 3 G-protein coupled

receptors (Pin and Duvoisin, 1995; Berghard and Buck, 1996; Runnenburger *et al.*, 2002). **Figure 7** illustrates the difference in structure between the V1R and V2R receptors (Tirindelli *et al.*, 1998; Coutinho and Knopfel, 2002). V2R receptors are also associated with major histocompatibility complex molecules and β2-microglobulin, which together form a large multimeric receptor complex (Bigiani *et al.*, 2005; Leinders-Zufall *et al.*, 2004). Some ligands have been demonstrated to be associated with V1R receptors, such as farnesene and 2-heptanone (Boschat *et al.*, 2002), while no ligands are known for V2R receptors (Leinders-Zufall *et al.*, 2000).

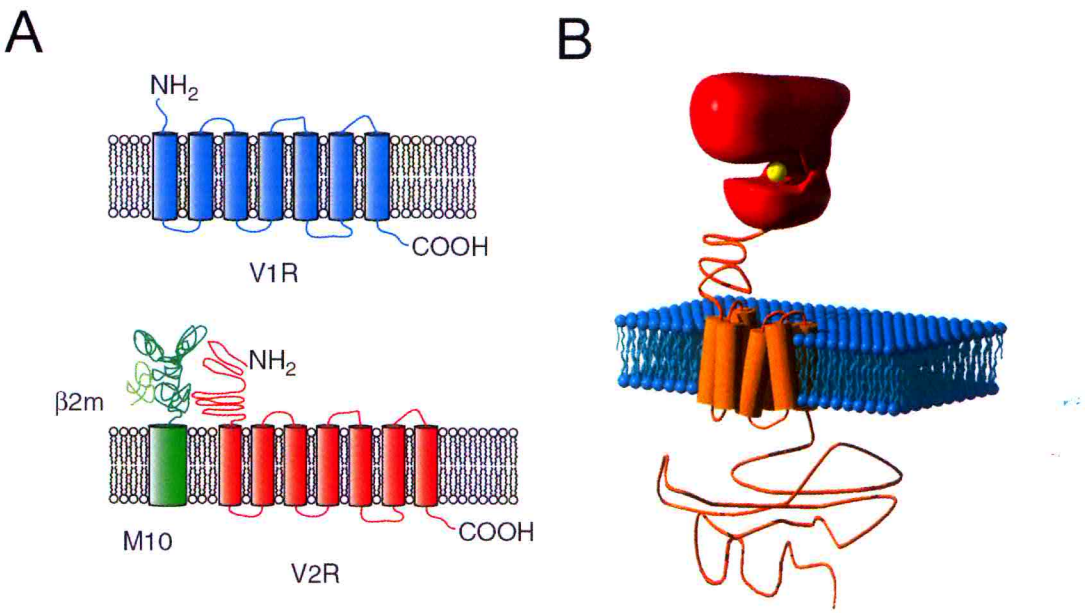

Figure 7. **A**) Diagram showing the general topology of V1R and V2R receptors. Both are seven transmembrane domain proteins. V2R receptors have a large 70 kDa extracellular N-terminal domain and form a multimeric complex with β2m and major histocompatibility complex molecule M10. **B**) The metabotropic glutamate receptor (shown) is thought to be similar in structure to V2R receptors, both of which belong to group 3 GPCRs. Modified from Tirindelli *et al.*, 1998 and Coutinho and Knopfel *et al.*, 2002.

Vomeronasal receptors, V1R and V2R, are also located in different areas of the vomeronasal organ. Apical neurons express the V1R type receptor while basal neurons express V2R type receptor, and hence it is common for these neurons to be referred to by their receptor type (i.e V2R neurons). In the sensory epithelium V1R (or apical) neurons are located closer to the luminal space and therefore typically have a shorter dendrite (<40 μm) while V2R (basal) neurons are located closer to the periphery of the organ, and therefore normally have a longer dendrite (>40 μm) (Fieni *et al.*, 2003). Dendrite length is also partially dependent on where the neuron is located within the sensory epithelium; neurons closer to the periphery have shorter dendrites as the sensory epithelium is narrower in that region. Axons from the V1R neurons terminate in the anterior AOB, while axons from V2R neurons terminate in the posterior AOB (Halpern *et al.*, 1998; Brennan and Keverne, 2004) (**Figure 8**). Information is then projected from the AOB to the completely overlapping regions in the bed nucleus of the stria terminalis (BNST), bed nucleus of the accessory olfactory tract (BAOT), medial amygdala (MeA), and the posteromedial cortical nucleus (PMCo); all of which are structures associated with the hypothalamus and amygdala which control hormonal levels and instinctive behaviors (Rodriguez, 2003; Brennan and Keverne, 2004).

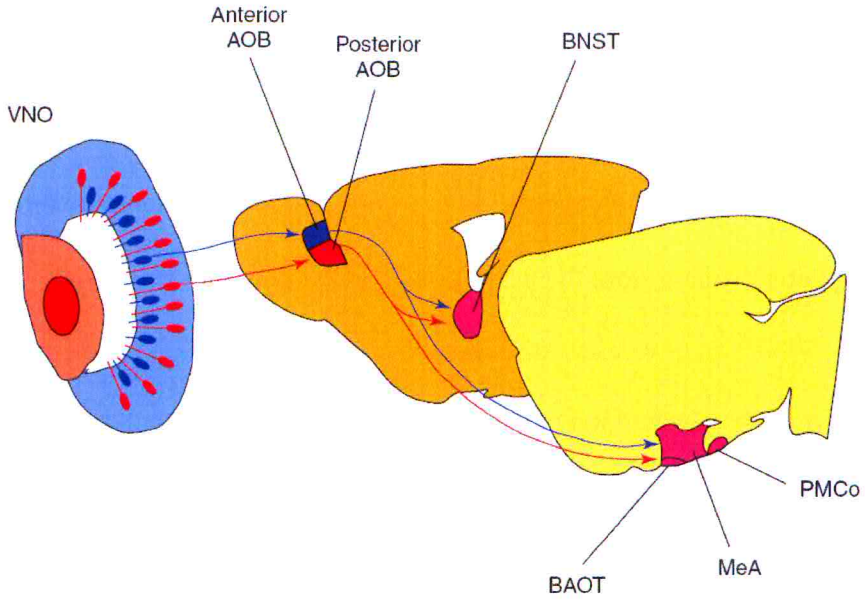

Figure 8. The vomeronasal organ and its connectivity to higher brain centers. V1R neurons project axons to glomeruli in the anterior AOB while V2R neurons project axons to the posterior AOB. Information then converges in completely overlapping interneuronal connections which take information from the AOB to the bed nucleus of the stria terminalis (BNST), bed nucleus of the accessory olfactory tract (BAOT), medial amygdala (MeA), and the poteromedial cortical nucleus (PMCo) of the amygdala. Adapted from Brennan and Keverne, 2004.

Information is transferred from the site of pheromone binding via a second messenger mediated transduction cascade. Pheromones bind specific membrane receptors (belonging to the more general class of V1R or V2R receptors), which activates a G protein mediated transduction cascade. The exact details remain unknown, but it is hypothesized that the G protein complex of Gβγ dissociates from the larger G protein complex activating phospholipase C which converts phosphatidyl inositol (PIP_2) into inositol triphosphate (IP_3) and diacylglycerol (DAG) (Runnenburger *et al.*, 2002). DAG has been shown to directly activate transient receptor potential channel 2 (TRP2) which

allows the influx of cations, namely Ca^{+}, and subsequent depolarization of the cell membrane (**Figure 9**) (Liman *et al.*, 1999; Rodriguez, 2003; Lucas *et al.*, 2003). IP_3 has has also been shown to effect current response in VSNs, however it is unclear if IP_3 represents a primary step in the activation of transduction conductance or more likely an event further downstream from the activation of TRP2 channels (Inamura *et al.*, 1997; Lucas *et al.*, 2003). In any case, once depolarization is initiated, it is propagated along the dendrite by voltage gated ion channels resulting in action potentials and the transfer of information to higher cortical areas.

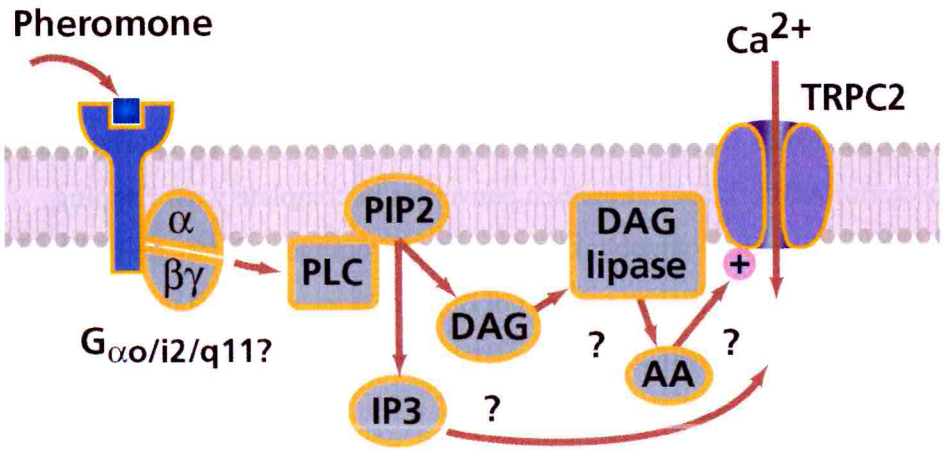

Figure 9. Proposed pheromone transduction cascade. Pheromones bind a V1R or V2R receptor which is coupled to a G-protein. Part of the G-protein complex dissociates and activates phospholipase C (PLC) which hydrolyses phosphatidyl inositol (PIP2) into diacylglycerol (DAG) and inositol triphosphate (IP3). DAG lipase may convert DAG into arachidonic acid (AA), but more recent evidence has shown that DAG can act directly on transient receptor potential channels (TRPC2). The role of IP3 and AA has not been solidified. Adapted from Rodriguez, 2003.

While the cascade is not certain, the role of TRP2 has been solidified by experiments where the TRP2 channel gene has been knocked out. The resulting transgenic mice show ablation of the wildtype male aggression to intruder males and, in females, elimination of maternal aggression to intruder males (Stowers *et al.*, 2002; Leypold *et al.*, 2002). These two behaviors are also eliminated if the VNO is completely ablated, while there is no difference in the main olfactory function. Sexual behavior is also reduced in VNO ablated animals, however, sexual behavior is unaltered in TRP2 deficient animals suggesting that there may be more than one pathway mediating pheromone transduction (Wysocki and Lepri, 1991; Leypold *et al.*, 2002; Stowers *et al.*, 2002).

The coding of information from the VNO seems to differ from the main olfactory system where odors appear to use a combinatorial receptor coding (Firestein, 2001). Data from calcium imaging experiments, where it was observed that each ligand activates a unique, nonoverlapping subset of VSNs, suggests that VSNs are tuned to recognize one or perhaps very few pheromonal components, where increasing concentration did not activate more neurons (Leinders-Zufall *et al.*, 2000). Based on the calcium imaging data, Luo and Katz (2004) have proposed a simple labeled lines strategy, known as the "one cell – one ligand – one receptor" model which is also supported by the observation that tagging a VSN with a marker for a particular receptor labels a very small fraction of VSNs (about 300 neurons or ~1% of the total number of VSNs (Luo and Katz, 2004; Rodriguez *et al.*, 1999).

The electrophysiology of voltage gated ion channels in vomeronasal sensory neurons has been studied in dissociated cell preparations from frog (Trotier and Doving, 1996), mouse (Liman and Corey, 1996), lizard (Labra *et al.*, 2005), hamster (Liman, 2003), rat (Trotier *et al.*, 1998), and in slice preparations from turtle (Taniguchi *et al.*, 1996), snake (Taniguchi *et al.*, 2000) and rat (Inamura *et al.*, 1997). These studies have shown that VSNs have TTX sensitive Na^+ channels and TEA sensitive K^+ channels which are primarily responsible for action potential firing in addition to other modulatory voltage gated ion conductances. Until now, no electrophysiological studies in acute slice preparations from the murine VNO have been published.

In this study, we examine the electrophysiological properties of a novel acute VNO slice preparation from the mouse and create a model of the electrical activity of the VSN based on our findings. Since we were interested primarily in the generation of action potentials and the overall firing behavior of VSNs, we concentrated on the study and modeling of voltage gated Na^+ and K^+ ion conductances.

MATERIALS AND METHODS

Acute Slices of the Vomeronasal Organ

Adult (30-90 days old) 129/Sv mice were used for the preparation of acute VNO slices. Mice were asphyxiated with CO_2 and the VNO was removed and rinsed in chilled Ringer's solution (**Figure 10A** and **B**). The capsule and all cartilaginous tissue were carefully removed and the two halves of the VNO were extracted from the vomer bone (**Figure 11**). Each half of the VNO was then separately treated. The VNO was embedded in 0.5% low grade agar (Cat# A7002-250G, Sigma, St. Louis, MO, USA) prepared with 0.9% saline solution once the agar had cooled to ~38°C, just prior to solidification (**Figure 12**). Upon solidification, the agar block was fixed in a glass Petri dish – orienting the VNO perpendicular to the blade - in preparation for slicing with a vibratome (Vibratome 1000 Plus Sectioning System, St. Louis, MO, USA). Coronal cross-sections of the VNO 250 μm in thickness were cut using a Teflon coated blade (Personna, American Safety Razor Company, VA, USA) in bubbled artificial cerebral spinal fluid (ACSF). Slices, embedded in their agar support, were then left to recover for >30 minutes before electrophysiological experiments were initiated (**Figure 13A**). Even after 5 hours of incubation, the blood vessel of the VNO was seen to be expanding and contracting suggesting that the slice was still alive after this time (**Figure 13B**).

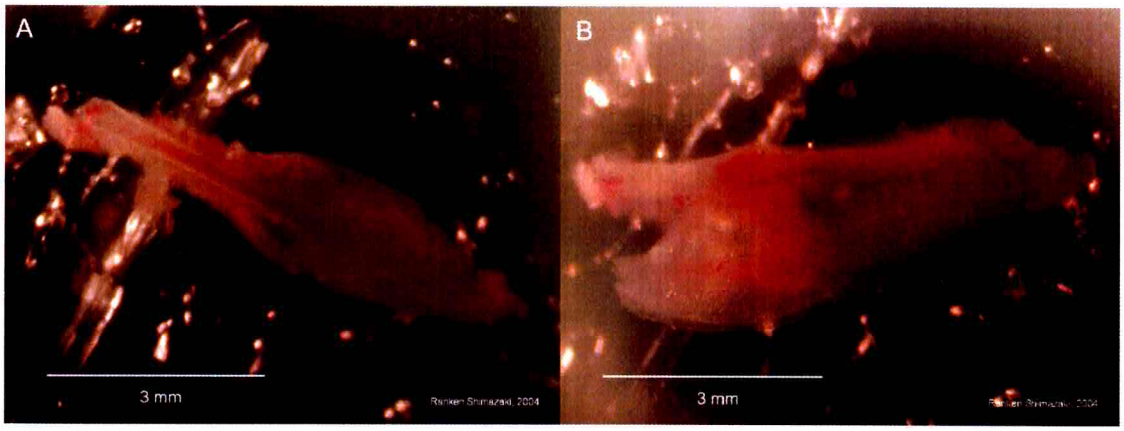

Figure 10. The intact, capsule encased, vomeronasal organ freshly extracted from the mouse. **A**) The bilateral organization of the VNO. **B**) The vomer bone and cartilaginous tissue are clearly visible.

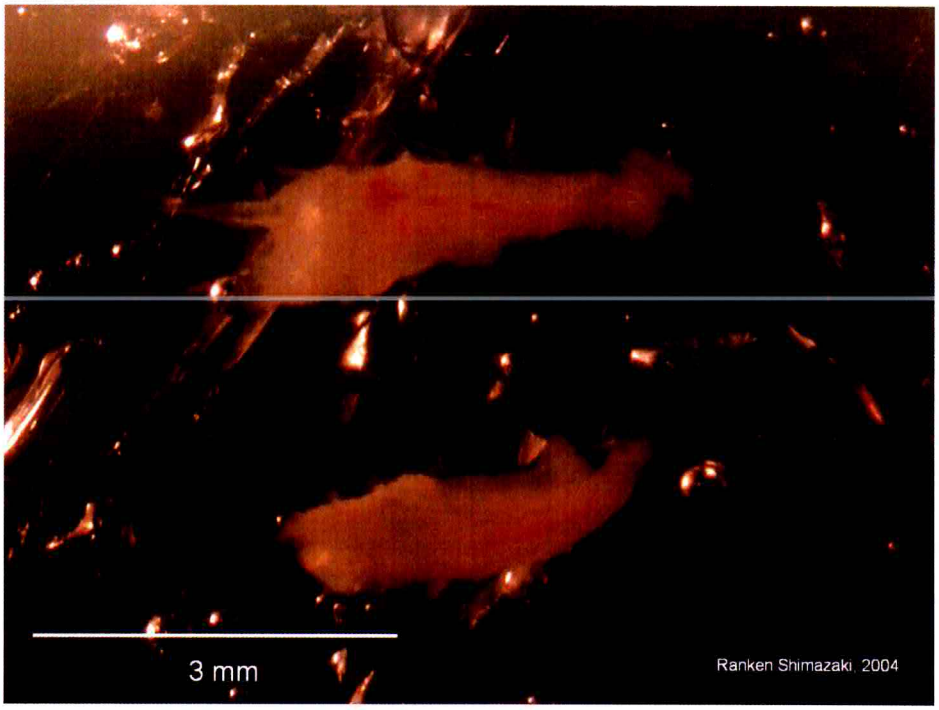

Figure 11. The vomeronsal organ dissected from the capsule and vomer bone. The blood vessel can be seen running the length of the organ.

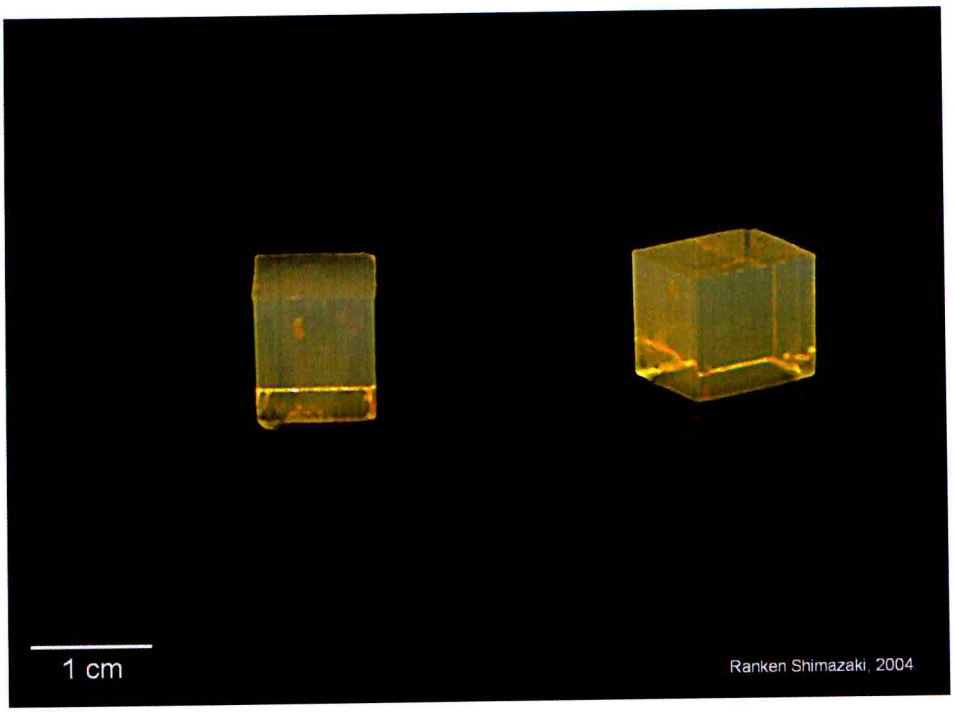

Figure 12. Each half of the vomeronasal organ is embedded in an agar block vertically and perpendicular to the anticipated blade axis in preparation for sectioning.

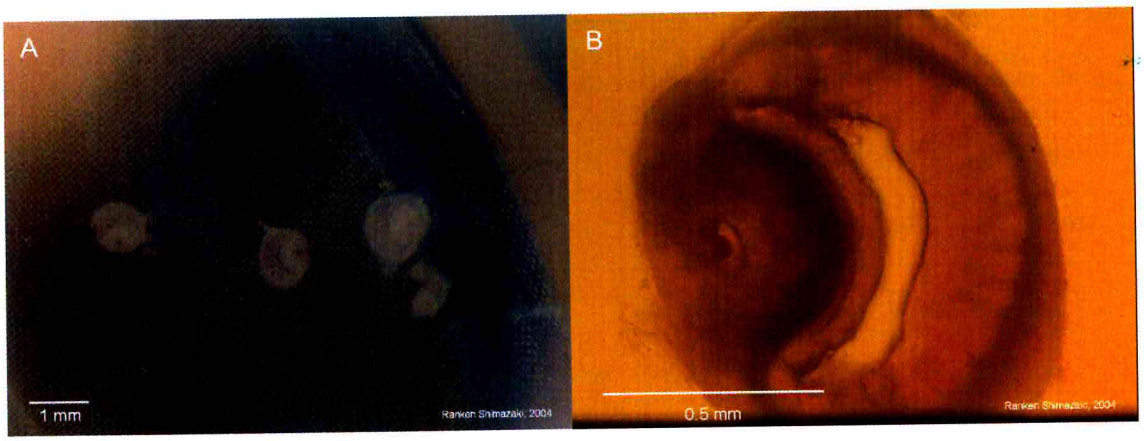

Figure 13. **A**) 250 μm thick slices of the vomeronasal organ with surrounding agar support. **B**) The morphology of the VNO remains intact within the slice, where the blood vessel, luminal space, and sensory epithelium are clearly visible. Refer to **Figure 4** for complete structural labeling.

Electrophysiological Recordings

An upright microscope (Olympus BX51WI; Tokyo, Japan) was used to visualize the slice preparation using bright field optics and fluorescence (Olympus U-RFL-T mercury lamp) at 40x. The recording chamber was continuously perfused with bubbled ACSF by gravity flow. The slice was anchored to the base of the chamber using a home-made U shaped platinum wire fitted with nylon threads ~3 mm apart from one another, thereby holding down the agar support without touching the slice itself.

The whole-cell patch clamp technique was used under voltage clamp and current clamp configurations using a Multiclamp 700B amplifier (Axon Instruments, La Jolla, CA, USA). **Figure 14A** shows a V2R neuron tagged with EGFP in the slice preparation under UV excitation. **Figure 14B** shows the same frame shown in **A** but in transmission mode and also shows the patch electrode. **Figure 14C** shows the VSN and electrode (filled with fluorescein) under blue light excitation. **Figure 14D** shows three V2R neurons in the slice preparation expressing EGFP excited with blue light.

A Digidata 1200 analog to digital converter was used to interface the amplifier with a PC running pClamp 9.2 (Axon Instruments). Currents and voltage signals were low-pass filtered at 10 and 1 kHz and sampled at 20 and 10 kHz. Pipettes were pulled from glass capillaries (PG10165-4, World Precision Instruments, Sarasota, FL, USA) using a 2 stage Narishige puller (model PP-830, Narishige, Tokyo, Japan). Pipettes had a typical bath resistance of 3-6 MΩ and GΩ seals were obtained without fire polishing. Whole-cell

recordings were obtained from patching the soma of basal vomeronasal sensory neurons located on the surface of VNO slices. Resting membrane potential was measured as the potential at which the current was zero.

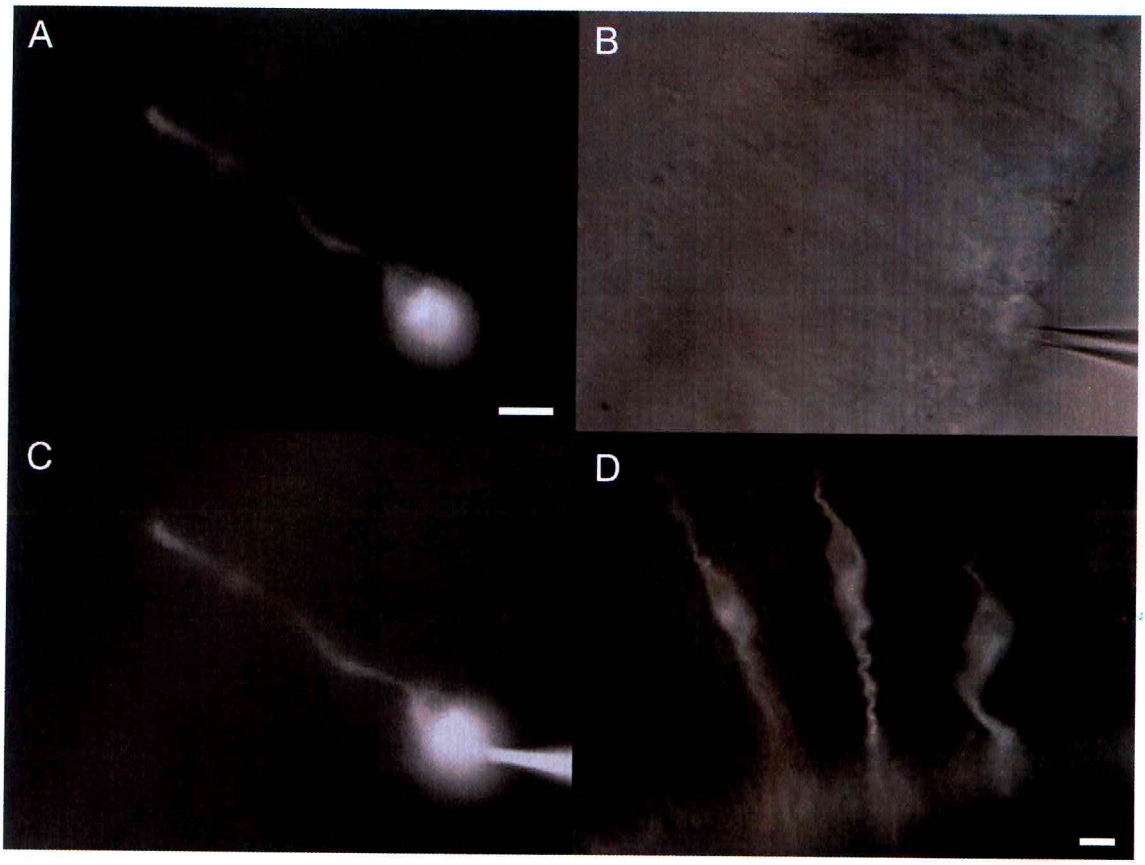

Figure 14. Vomeronasal sensory neurons. **A**) Basal (V2R) vomonasal sensory neuron expressing EGFP. **B**) Transmission photograph of the sensory epithelium showing the same cell as in **A**. **C**) As A but showing the pipette illuminated with fluorescein. The scale bar is 10 μm and is the same for **A-C**. **D**) EGFP labeled V2R neurons in the sensory epithelium showing clear axonal projections towards the top of the frame and dendrites extending towards the bottom of the frame. Scale bar is 10 μm. For all fluorescence images excitation light was 460-490 nm and emission was long-pass filtered (>510 nm).

Input resistance was measured as the slope of linear current-voltage relationship around -80 mV. Cell membrane capacitance was measured by integrating the capacitive current transient elicited by a 10 mV hyperpolarizing step from a holding potential of –60 mV (Bigiani and Roper, 1993; Vogalis *et al.*, 2005). Series resistance and junction potential were not corrected. All experiments were conducted at room temperature 20-23°C.

Data analysis was performed using Pclamp 9.2 software (Axon Instruments) and Igor 4.0 software (Wavemetrics, OR, USA) Data are given as mean ± standard deviation and the total number of observations (n).

Recording Solutions

The intracellular recording solution contained the following: 145 mM KCl, 4 mM $MgCl_2$, 10 mM HEPES, 0.5 mM EGTA, 1 mM ATP and 0.1 mM GTP. The extracellular solution was standard ACSF solution containing: 125 mM NaCl, 26 mM $NaHCO_3$, 1.25 mM NaH_2PO_4, 2.5 mM KCl, 1.0 mM $MgCl_2$, 2.0 mM $CaCl_2$, 4.5 mM glucose, bubbled with 5% CO_2 to reach a pH of 7.4. Some recordings were made with the addition of 1 μM TTX (Tocris, Ellisville, MO) or 10 mM TEA to the extracellular solution as indicated. All chemicals were from Sigma (Sigma, St. Louis, MO) unless otherwise stated.

Model

All the simulations were carried out with the NEURON simulation program v5.7 (Hines and Carnevale, 1997) using its variable time step feature. A generic vomeronasal neuron was implemented with a somatic compartment (14x14μm) and a 70μm long dendrite with a 1.5μm diameter. Uniform passive properties were used, with Ra = 150 Ω·cm, Rm = 155 kΩ·cm^2, and τm = 155ms. Resting potential was set at -70mV and temperature at 22°C. The firing pattern of VNO neurons was simulated by solving the following equation:

$$Cm\frac{dV}{dt} = \frac{V - Vrest}{Rm} + I_{Na}(V,t) + I_K(V,t) + I_{inj}(t) \qquad (1)$$

where V is the membrane potential, Cm is the specific membrane capacitance, *Vrest* is the resting potential for firing VNO neurons, t is the time, I_{Na} and I_K are the Na^+ current and K^+ current, respectively, I_{inj} is the injected current and R_m is the specific membrane resistance.

The ionic current (I_x where x = Na^+ or K^+) was implemented using an Hodgkin-Huxley (HH) like formalism (Johnston and Wu, 1995) using the following equation:

$$I_x = \bar{g}_x m^n h(V - E_x) \qquad (2)$$

where $\bar{g}_x$ is the specific maximum conductance and E_x is the reversal potential. Voltage dependent parameter *m* is the activation gating particle and *h* is the inactivation gating particle. We will refer to *y* as the general gating particle. Initially we define $y = y_\infty$ and at subsequent time steps as follows:

$$\frac{dy}{dt} = \frac{y_\infty - y}{\tau_y} \qquad (3)$$

The steady-state voltage dependence of the general gating particle *y* was implemented using a simple Boltzman function,

$$y_\infty = \frac{1}{1 + \exp^{\frac{V_y - V}{k_y}}} \qquad (4)$$

for activation ($y = m$) and is defined as

$$y_\infty = 1 - \frac{1}{1 + \exp^{\frac{V_y - V}{k_y}}} \qquad (5)$$

for inactivation ($y=h$) where, in both cases, V_y is the voltage at which point y_∞ is 0.5, k_y is the slope of the sigmoid.

The time constant to reach steady-state was implemented using the arbitrary bell-shaped function

$$\tau_y = \frac{\exp^{z_y \gamma_y (V - V_{1/2y})}}{a_{0y} \cdot (1 + \exp^{z_y (V - V_{1/2y})})} \quad (6)$$

where a_{0y} defines the maximum amplitude of τ_y, z_y affects the width of the curve, and γ_y affects the degree of curve symmetry defined by τ_y, and $V_{1/2y}$ defines where on the time axis the curve appears (i.e. controls horizontal shift). It is important to note that, unlike the HH model, the time constant, τ, is decoupled from the steady-state kinetics.

Refer to **Table 1** (pg. 35) for a list of parameter values used.

RESULTS AND DISCUSSION

The goal of this study was to experimentally measure firing activity of vomeronasal sensory neurons in acute slice preparations and to estimate model parameters that produce an accurate simulation of the input-output characteristics (firing rate as a function of input current). A model that reproduces the effective firing behavior of vomeronasal sensory neurons in response to current steps by taking into account the sodium and potassium currents is proposed.

Slice Preparation

The novel murine slice preparation described in the methods section maintained the VNO cross-sectional structure. Slices were judged to be healthy by the continued expansion and contraction of the organ's blood vessel which persisted even after 5 hours in bubbled ACSF solution. Vomeronasal sensory neurons on the surface of the slice preparation were easily accessible to patch-clamp recording. Cells below the surface were much more difficult to reach as the sensory epithelium has an elastic consistency.

Electrophysiological recordings from acute slice preparations from the vomeronasal organ have several advantages and disadvantages with respect to isolated vomeronasal sensory neurons.

Voltage clamp recordings from relatively large cells with long processes, such as VSNs, are inevitably more prone to the problem of inadequate space clamping. In slices, this problem is even more pronounced where the cellular structure and plasma membrane specializations remain intact and therefore more complex compared to isolated cells which tend to shrink and become more round over time. Cells in slice preparation may also be electrically coupled which would introduce other factors such as larger apparent cytoplasmic volumes. While VSNs are accessible to patch-clamp recordings in slice preparations, it is still easier to obtain whole-cell recordings from cleanly isolated cells.

Despite these drawbacks to slice preparations, they also present many advantages. Since the cells are in a more native state, the majority of their connections are preserved. Because there is no dissociation procedure, no enzymes are used which could alter the native cellular response. In addition, once a seal is achieved it is possible to record for long times (2+ hours) from a single VSN in the slice preparation.

Passive Properties

The electrophysiological properties of mouse vomeronasal sensory neurons in slices were investigated by using the whole-cell patch-clamp technique as described in the methods section. The resting potential (V_r) of the neurons ranged from -50 to -70 mV, averaging -63 ± 6 mV (n=16). In a few cells, spontaneous firing activity was observed at 0 current injection and some cells showed fluctuation in resting potential (±5mV).

The average capacitance C_m was 12 ± 5 pF (range: 4 to 21 pF, n=16). The average input resistance (R_i) was 7 ± 5 GΩ (n=16) with a range between 1 and 18 GΩ . Since seal resistances are usually a few GΩ (with occasional higher values up to 50 GΩ), and therefore, are similar to the input resistance, in most recordings R_i is likely to underestimate the real membrane resistance (R_m) (Schild, 1989; Schild and Restrepo, 1998; Lynch and Barry, 1991; Lynch and Barry, 1989). Therefore it is likely that R_m is closer to the higher measured value of 18 GΩ rather than to the mean value.

Firing Behavior as a Function of Current Injection

The firing behavior of VSNs from slice preparations was studied though current clamp whole-cell patch clamp recordings. As shown in **Figure 15A** vomeronasal sensory neurons fired repetitive action potentials with current injections of only 2 pA. Increasing the current intensity increased the number of spikes. The firing frequency was plotted as a function of current intensity in **Figure 15B** and was fitted by a Michaelis-Menten equation (n=4).

The spike duration varied between cells averaging 15 ± 5 ms and ranging between 7 and 22 ms (n=9). In about half of the cases, tonic firing behavior was lost over time at high current injections. In these cases, the interspike interval was used to calculate the firing frequency. In some cases (n=7) cells showed no tonic activity, firing only 1 spike irrespective of the amount of current applied.

In other cells, spontaneous firing activity was observed at 0 current injection. This is likely related to the high sensitivity of VSNs where a current injection of only 1 or 2 pA is sufficient to stimulate a sustained train of action potentials. This can be attributed to the high input resistance that we observed in VSNs and the resting potential (-63 ± 6 mV) close to the threshold of action potential firing (-50 to -60 mV). The steady trains of action potentials generated by VSNs with little sign of adaptation, in contrast to olfactory receptor neurons, is in agreement with other studies on VNO neurons (Liman and Corey, 1996).

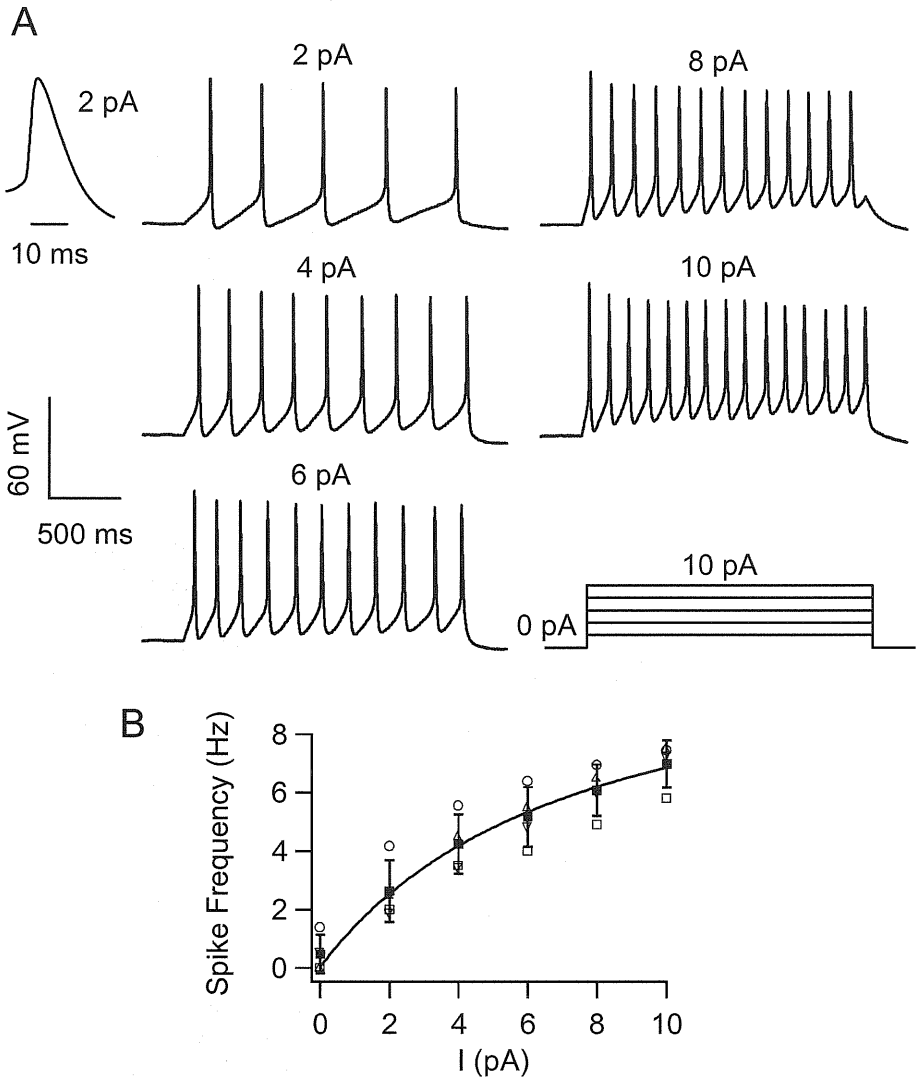

Figure 15. Firing patterns of vomeronasal sensory neurons from a VNO slice. **A**) Typical current-clamp responses to current injections of 2 to 10 pA for 2 seconds. In this cell, the resting potential (measured at 0 pA current injection) was -70 mV. The firing frequency increased as a function of injected current. The inset shows a single action potential upon 2 pA current injection at an expanded time scale. **B**) Firing frequency as a function of current injection for 4 neurons. Each neuron is represented by a different symbol. The black squares show the average ± standard deviation. The line is the best fit of the Michaelis-Menten equation $F=F_mI/(I+I_o)$ to the data with F_m=12 Hz, I_o=7.5 pA.

Voltage Gated Currents

To model the firing properties, voltage-gated conductances were investigated by voltage-clamp recordings of vomeronasal sensory neurons in situ, and an estimate of initial values for model parameters was obtained. The goal of this study was to obtain a simple model with the minimum number of parameters necessary to reproduce the electrical activity of vomeronasal sensory neurons, and therefore a detailed pharmacological analysis to separate different current components was not attempted. As previously shown in dissociated vomeronasal sensory neurons, the voltage-gated inward current is primarily a sodium current, composed both of a TTX-sensitive and a TTX-insensitive component (data not shown), although calcium currents are also present (Fieni *et al.*, 2003; Liman and Corey, 1996). The voltage-gated outward current was also composed of more than one component as it has been shown that TEA did not completely block the current. Our data were in general agreement with earlier findings from dissociated vomeronasal sensory neurons (Dean *et al.*, 2004; Fieni *et al.*, 2003; Liman and Corey, 1996; Trotier *et al.*, 1998).

Voltage Gated Inward Currents

Voltage dependent currents were studied in order to understand the mechanics of the neuronal firing activity. For activation, inward currents were elicited by applying depolarizing voltage steps of 50 ms duration from the holding potential to a test potential between -60 to +35 mV (**Figure 16A**). Large inward Na^+ currents and outward K^+

currents can be seen. Peak currents at each voltage were measured and plotted in **Figure 16B** as a function of the test potential for two holding potentials, -70 mV or –60 mV. The peak of the Na^+ current appeared between -20 and -25 mV, and was partially dependent on the holding potential, shifting towards more negative values as the holding potential decreased. Na^+ currents were sensitive to TTX, however ~13% of the inward current (measured at -15 mV) remained after TTX suggesting that there is also a TTX insensitive component (data not shown).

Figure 16C shows the steady-state activation curve where the calculated normalized conductances were plotted as a function of voltage. The activation parameters that were subsequently used as initial values in the model, were estimated by fitting the data with the following equation:

$$\frac{g_{Na}(V)}{g_{Na\max}} = \frac{1}{\left(1+\exp^{\frac{V_m - V}{k_m}}\right)^n} \qquad (7)$$

where $g_{Na\max}$ is the maximum sodium conductance, V_m is the half activation potential, k_m is a slope constant, and n = 3 (see equation in the model). At a holding potential of -70 mV the average V_m was -44.7 ± 12.1 mV and k_m was 3.7 ± 2.1 mV (n=3), similar values were obtained at -60 mV, where the average was -42.5 ± 4.7 mV and k_m was 5.7 ± 2.5 mV (n=20). Changing the holding potential does not affect the rate (k_m) of Na^+ current activation, nor does it seem to drastically affect the voltage at which half of the channels are open (V_m).

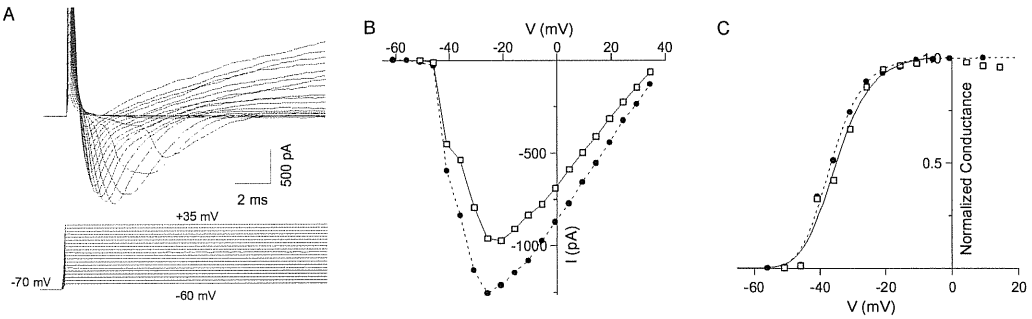

Figure 16. Activation properties of inward currents. **A**) Voltage-clamp recordings from a vomeronasal neuron from a VNO slice. Current traces measured as the voltage was stepped in increments of 5 mV from -60 mV to +35 mV from a holding potential of -70 mV. **B**) Current-voltage relationships of the peak inward currents measured in the same neuron at the holding potential of –70 mV (circles) or –60 mV (squares). **C**) Steady-state activation curve. Normalized conductances from data in **B** were plotted as a function of voltage. Activation curves were fit with equation (7) . At the holding potential of –70 mV, broken line, V_m= – 44.6 mV, k_m = 6 mV. At the holding potential of –60 mV, continuous line, V_m= – 43.9 mV, k_m = 6.7 mV at –60 mV.

To measure the inactivation properties of the sodium channels the steady-state voltage-dependence of inactivation was estimated by using a two-pulse protocol, as shown in **Figure 17A**. First, the neuron was held for 300 ms at voltages from –100 to –20 mV to achieve steady-state inactivation of sodium channels, and then a test pulse to 0 mV was given to elicit the residual current that had not been inactivated. Peak currents were normalized to the maximal value and plotted as a function of the pre-pulse voltage to give the steady-state inactivation curve shown in **Figure 17B**. The inactivation parameters were estimated by fitting the data with the following equation:

$$\frac{I(V)}{I_{\max}} = \frac{1}{\left(1+\exp^{\frac{V-V_h}{k_h}}\right)} \qquad (8)$$

where I_{max} is the maximal peak current, V_h is the half activation potential and k_h is the slope constant. The average V_h was -56.2 ± 7.2 mV and k_h was 8.9 ± 2.3 mV (n=14). The kinetics of activation and inactivation of sodium currents were fit by a single exponential and found to be very fast: at 0 mV the time constants of activation and inactivation were 0.5 and 1 ms, respectively.

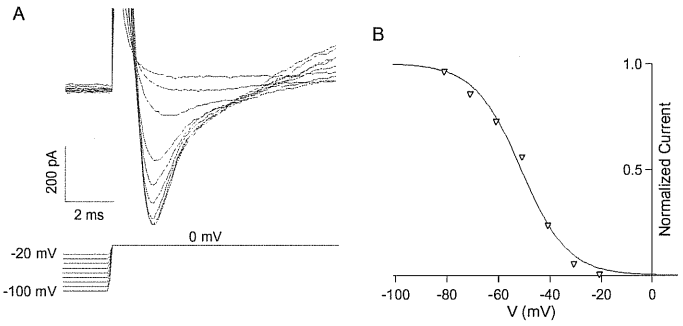

Figure 17. Inactivation properties of inward currents. **A**) Inward currents elicited by a test pulse of 0 mV following the application of a 300 ms pre-pulse at the voltages indicated. **B**) Peak currents were normalized to the maximal current and plotted as a function of the pre-pulse potential. The inactivation curve was fit using equation (8) with $V_h = -51.1$ mV, $k_h = 9.0$ mV.

Voltage Gated Outward Currents

Properties of outward currents were estimated as shown in **Figure 18**. Currents in response to step depolarizations of 400 ms duration from a holding potential of –60 mV are shown in **Figure 18A**. The outward currents showed little inactivation over 400 ms. Peak outward currents and normalized conductances were plotted as a function of voltage in **Figure 18B** and **C**, respectively. Like the Na^+ currents, the K^+ currents also activate between -40 and -50 mV but, unlike Na^+ currents, show no significant differences as a

function of holding potential. The maximum outward current was saturated beyond ~60 mV. The steady-state activation curve for potassium activation (**Figure 18C**) was fit with the equation:

$$\frac{g_K(V)}{g_{K\max}} = \frac{1}{\left(1+\exp^{\frac{V_m - V}{k_m}}\right)^n} \qquad (9)$$

where $g_{K\max}$ is the maximum potassium conductance, V_m is the half activation potential, k_m is a slope constant, and n=1.5. At a holding potential of -60 mV the average V_m was -21.0 ± 4.9 mV and k_m was 12.8 ± 2.4 mV (n=19).

Potassium activation currents were fit by a single exponential and were approximately an order of magnitude slower than those for sodium: at 0 mV the time constant of activation was 20 ms. Inactivation kinetics were further investigated with step depolarizations of 9 second duration (**Figure 18D**). Inactivation of outward currents was very slow and was unable to be fit by a single exponential function. Instead, a double exponential function provided an accurate description of inactivation showing a fast component (tau = ~0.8 s at 0 mV) and a slow component (tau = ~3 s at 0 mV) as seen in **Figure 18D**.

The K^+ current was largely abolished in the presence of 10 mM TEA, leaving an average of 32% (range 25% to 40%, n=4) of the original outward current (data not shown). This is in agreement with previous studies and suggests that there is likely more than one outward current responsible for repolarization, but that the majority is due to a TEA sensitive K^+ current (Liman and Corey, 1996).

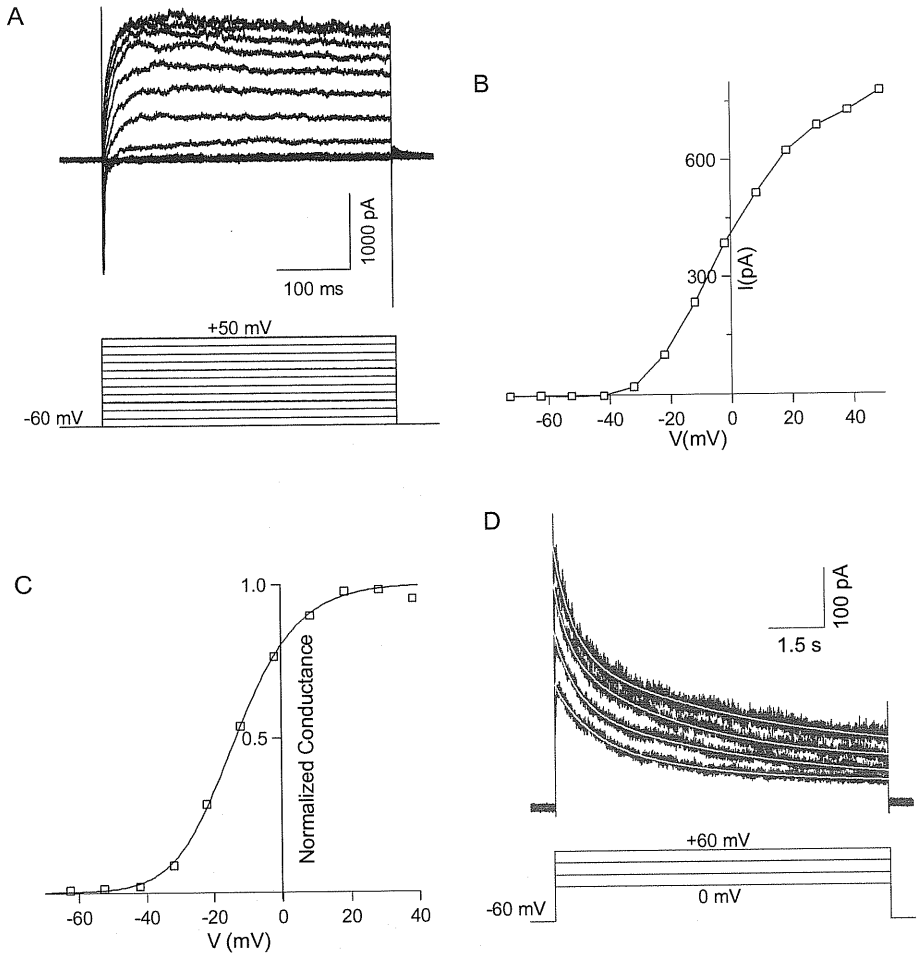

Figure 18. Activation and inactivation of outward currents. **A)** Currents elicited by 400 ms voltage steps of 10 mV from –50 to +50 mV from a holding potential of -60 mV. **B)** Current-voltage relationship of the peak outward currents. **C)** Outward current steady-state activation curve. Normalized conductances from data in **B** were plotted as a function of voltage. The activation curve was fit using equation (9) with V_m= – 18.8 mV, k_m = 10.2 mV. **D)** Inactivation of potassium current. Voltage steps of 9 second duration and 20 mV amplitude from 0 to +60 mV were applied from a holding potential of -60 mV. Solid white lines represent the fit of the data with a double exponential function with time constants of 0.8 s and 3 s for the fast and slow components at 0 mV, 0.6 s and 5 s at 20 mV, 0.4 s and 4 s at 40 mV, and 0.5 s and 5 s at 60 mV.

Model

We attempted to mimic the behaviour of VNO neurons using a simple paradigm: one type of Na^+ channel and one type of K^+ channel. We defined our neuron as described in the methods. Our experimental voltage clamp data was used as a starting point from which we made modifications to more closely match the firing behavior and current response to stimulation. Table 1 shows the final parameters used in the model.

Table 1. Model Parameters used to construct a model VNO neuron.

Parameter	Na^+	K^+
n	3	1.5
$\bar{g}_x$	11.4 mS/cm^2	2.1 mS/cm^2
E_x	50 mV	-75 mV
V_m	-42 mV	-21 mV
k_m	8 mV	12.8 mV
a_{0m}	0.3 ms^{-1}	0.003 ms^{-1}
$V_{1/2m}$	-38.9 mV	-75 mV
z_m	0.05	0.0002
γ_m	0.2	0.82
V_h	-60 mV	0 mV
k_h	2 mV	60 mV
a_{0h}	0.03 ms^{-1}	0.002 ms^{-1}
$V_{1/2h}$	-80 mV	-70 mV
z_h	0.09	0.05
γ_h	0.5	0.95

Differences between our experimentally determined parameters and those parameters used in the two channels defining our model were inevitable as our goal was to develop an effective model of VSN behavior. Hence, while the experimentally determined currents were of primary importance in action potential generation, other currents present

in real cells were not implemented and so the modifications to the model can be seen as a simplified representation of the holistic behavior of inward and outward currents. **Figure 19** shows a comparison between experimental and simulated voltage clamp recordings. As shown, the overall combined inward and outward currents in the model (**Figure 19B**), closely resemble those obtained experimentally (**Figure 19A**).

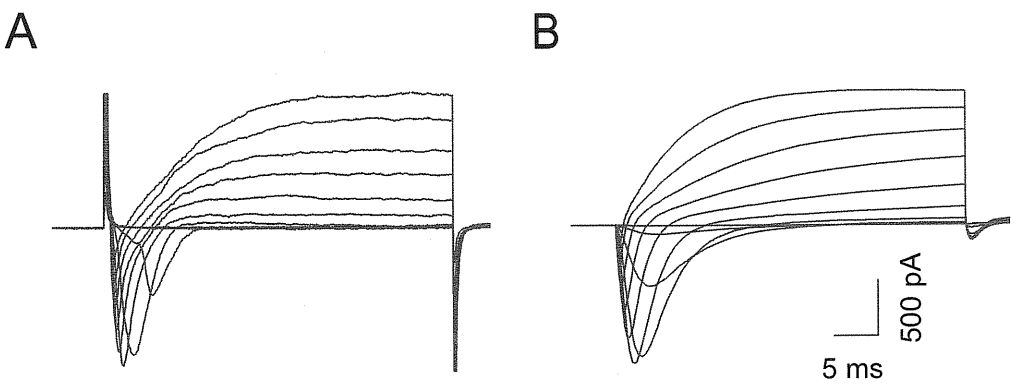

Figure 19. Experimental and simulated voltage-clamp recordings from a vomeronasal neuron. **A**) Currents measured experimentally. The holding potential was –70 mV and voltage was stepped from –60 to +30 mV in 10 mV increments, similar to the experiment shown in **Figure 16A**. **B**) Simulation of the same voltage-clamp experiment as shown in **A**.

Approaching the model from a behavioral standpoint, we placed the most emphasis on spike shape, amplitude, duration, and frequency – likely to be most important to the mouse as it relates to the coding of pheromonal signals. Using this framework, we were able to approximate the experimentally observed behavioral patterns (**Figure 20**), recreating a similar spike morphology (**Figure 20A**) and firing frequency (**Figure 20B**) in the VNO model.

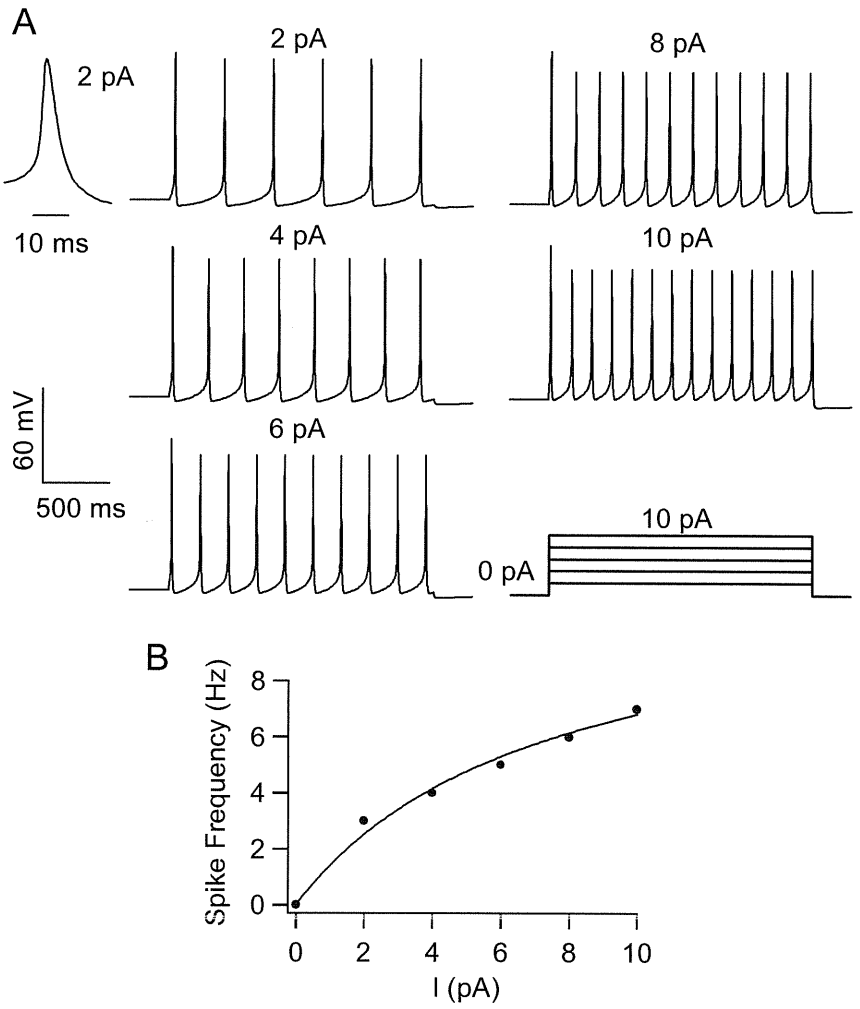

Figure 20. Simulated firing properties of the model vomeronasal neuron. **A**) The holding potential was set to –70 mV and the same type of experiment as shown in **Figure 15** was modeled. The firing frequency increased as a function of current injection in a manner similar to that observed experimentally. The inset shows the model of a single action potential upon 2 pA current injection at an expanded time scale. **B**) Firing frequency as a function of current injection calculated from the model. The simulated data were fit with a Michaelis-Menten equation $F=F_mI/(I+I_o)$ with $F_m=12$ Hz, $I_o=7.5$ pA as in the experimental recordings of **Figure 15**.

While there are discrepancies between the experimental data and our model due to our reduction of voltage dependent currents to two fundamental currents, they are few and apparently negligible as the overall firing behavior under current clamp conditions remains similar.

CONCLUSION

The slice preparation outlined here provides an excellent platform from which to study the electrophysiology of murine vomeronasal sensory neurons in a state close to that found natively in the animal.

The firing properties of VSNs closely resembled that of previous studies in dissociated cells and this study provides confirmation that VSNs, when in a more native state, behave similarly to dissociated neurons.

Modelling the effective behavior of vomeronasal sensory neurons suggests that while the gross behavior can be explained by a single Na^+ and single K^+ current, the exact spike morphology and firing pattern is dependent on more than these two currents. This model will be useful in the design of future experiments where the theories based on holistic firing behavior can be tested without animal sacrifice.

FUTURE DIRECTIONS

The obvious next step is the use of pheromones as a stimulant, instead of electric currents. This is somewhat complicated by the observation that any given VSN has only a single (or very, very few) receptor types located on its surface. Therefore, recording from a single VSN by patch-clamp recording may not be the best method for visualizing

pheromone induced responses. Instead multi-electrode recordings and/or imaging of calcium or voltage sensitive dye associated with VSNs will likely prove more practical.

This model was a first approximation of VSN behavior. It is obvious that while this model represents a good effective model, there is room for improvement through the experimental characterization and addition of other currents to the model.

ACKNOWLEDGMENTS

I would like to thank all those in the Menini lab who have contributed to this work and provided the knowledge base from which to work. More specifically I would like to thank Anna Boccaccio for all of her help ranging from practical experimental considerations to helping in my understanding of the biophysical theories underlying the bulk of this work. I would like to thank Andrea Mazzatenta for elucidating the anatomy of the VNO and Giulietta Pinato for time spent with me amidst a plethora of cables attached to the electrophysiological setup. The modeling was in large part accomplished through collaboration with Michele Migliore, whose hospitality in Palermo was second to none. Last, but not least, I would like to thank Anna Menini for all of her advice and encouragement throughout the course of this work (and outside the course of this work as well). I would also like to thank Juraj Rievaj for his attempts to teach me Czech and Simone Pifferi for not swearing directly at me . . . but slightly off to the side. I would also like to thank all those in the Torre lab with whom we share space, resources, and good times.

REFERENCES

Berghard,A. and Buck,L.B. (1996) *Sensory transduction in vomeronasal neurons: evidence for G alpha o, G alpha i2, and adenylyl cyclase II as major components of a pheromone signaling cascade.* J. Neurosci., 16, 909-918.

Bigiani,A., Mucignat-Caretta,C., Montani,G. and Tirindelli,R. (2005) *Pheromone reception in mammals.* Rev. Physiol Biochem. Pharmacol..

Bigiani,A. and Roper,S.D. (1993) *Identification of electrophysiologically distinct cell subpopulations in Necturus taste buds.* J. Gen. Physiol, 102, 143-170.

Boschat,C., Pelofi,C., Randin,O., Roppolo,D., Luscher,C., Broillet,M.C. and Rodriguez,I. (2002) *Pheromone detection mediated by a V1r vomeronasal receptor.* Nat. Neurosci., 5, 1261-1262.

Brennan,P.A. (2001) *The vomeronasal system.* Cell Mol. Life Sci., 58, 546-555.

Brennan,P.A. and Keverne,E.B. (2004) *Something in the air? New insights into mammalian pheromones.* Curr. Biol., 14, R81-R89.

Ciges,M., Labella,T., Gayoso,M. and Sanchez,G. (1977) *Ultrastructure of the organ of Jacobson and comparative study with olfactory mucosa.* Acta Otolaryngol., 83, 47-58.

Coutinho,V. and Knopfel,T. (2002) *Metabotropic glutamate receptors: electrical and chemical signaling properties.* Neuroscientist., 8, 551-561.

Dean,D.M., Mazzatenta,A. and Menini,A. (2004) *Voltage-activated current properties of male and female mouse vomeronasal sensory neurons: sexually dichotomous?* J. Comp Physiol A Neuroethol. Sens. Neural Behav. Physiol, 190, 491-499.

Doving,K.B. and Trotier,D. (1998) *Structure and function of the vomeronasal organ.* J. Exp. Biol., 201 (Pt 21), 2913-2925.

Dulac,C. and Axel,R. (1995) *A novel family of genes encoding putative pheromone receptors in mammals.* Cell, 83, 195-206.

Dulac,C. and Torello,A.T. (2003) *Molecular detection of pheromone signals in mammals: from genes to behaviour.* Nat. Rev. Neurosci., 4, 551-562.

Fieni,F., Ghiaroni,V., Tirindelli,R., Pietra,P. and Bigiani,A. (2003) *Apical and basal neurones isolated from the mouse vomeronasal organ differ for voltage-dependent currents.* J. Physiol, 552, 425-436.

Firestein,S. (2001) *How the olfactory system makes sense of scents.* Nature, 413, 211-218.

Halpern,M., Jia,C. and Shapiro,L.S. (1998) *Segregated pathways in the vomeronasal system.* Microsc. Res. Tech., 41, 519-529.

Halpern,M. and Martinez-Marcos,A. (2003) *Structure and function of the vomeronasal system: an update.* Prog. Neurobiol., 70, 245-318.

Herrada,G. and Dulac,C. (1997) *A novel family of putative pheromone receptors in mammals with a topographically organized and sexually dimorphic distribution.* Cell, 90, 763-773.

Hines,M.L. and Carnevale,N.T. (1997) *The NEURON simulation environment.* Neural Comput., 9, 1179-1209.

Holy,T.E., Dulac,C. and Meister,M. (2000) *Responses of vomeronasal neurons to natural stimuli.* Science, 289, 1569-1572.

Inamura,K., Kashiwayanagi,M. and Kurihara,K. (1997) *Inositol-1,4,5-trisphosphate induces responses in receptor neurons in rat vomeronasal sensory slices.* Chem. Senses, 22, 93-103.

Jacobson,L., Trotier,D. and Doving,K.B. (1998) *Anatomical description of a new organ in the nose of domesticated animals by Ludvig Jacobson (1813).* Chem. Senses, 23, 743-754.

Johnston,D. and Wu,S.M. (1995) Foundations of cellular neurophysiology. MIT Press, Cambridge, Mass.

Keverne,E.B. (2000) *Neuroendocrinology briefings 11: pheromones and reproduction.* J. Neuroendocrinol., 12, 1045-1046.

Labra,A., Brann,J.H. and Fadool,D.A. (2005) *Heterogeneity of voltage- and chemosignal-activated response profiles in vomeronasal sensory neurons.* J. Neurophysiol..

Leinders-Zufall,T., Brennan,P., Widmayer,P., PC,S., Maul-Pavicic,A., Jager,M., Li,X.H., Breer,H., Zufall,F. and Boehm,T. (2004) *MHC class I peptides as chemosensory signals in the vomeronasal organ.* Science, 306, 1033-1037.

Leinders-Zufall,T., Lane,A.P., Puche,A.C., Ma,W., Novotny,M.V., Shipley,M.T. and Zufall,F. (2000) *Ultrasensitive pheromone detection by mammalian vomeronasal neurons.* Nature, 405, 792-796.

Leypold,B.G., Yu,C.R., Leinders-Zufall,T., Kim,M.M., Zufall,F. and Axel,R. (2002) *Altered sexual and social behaviors in trp2 mutant mice.* Proc. Natl. Acad. Sci. U. S. A, 99, 6376-6381.

Liman,E.R. (2003) *Regulation by voltage and adenine nucleotides of a Ca2+-activated cation channel from hamster vomeronasal sensory neurons.* J. Physiol, 548, 777-787.

Liman,E.R. and Corey,D.P. (1996) *Electrophysiological characterization of chemosensory neurons from the mouse vomeronasal organ.* J. Neurosci., 16, 4625-4637.

Liman,E.R., Corey,D.P. and Dulac,C. (1999) *TRP2: a candidate transduction channel for mammalian pheromone sensory signaling.* Proc. Natl. Acad. Sci. U. S. A, 96, 5791-5796.

Lucas,P., Ukhanov,K., Leinders-Zufall,T. and Zufall,F. (2003) *A diacylglycerol-gated cation channel in vomeronasal neuron dendrites is impaired in TRPC2 mutant mice: mechanism of pheromone transduction.* Neuron, 40, 551-561.

Luo,M. and Katz,L.C. (2004) *Encoding pheromonal signals in the mammalian vomeronasal system.* Curr. Opin. Neurobiol., 14, 428-434.

Lynch,J.W. and Barry,P.H. (1989) *Action potentials initiated by single channels opening in a small neuron (rat olfactory receptor).* Biophys. J., 55, 755-768.

Lynch,J.W. and Barry,P.H. (1991) *Properties of transient K+ currents and underlying single K+ channels in rat olfactory receptor neurons.* J. Gen. Physiol, 97, 1043-1072.

Matsunami,H. and Buck,L.B. (1997) *A multigene family encoding a diverse array of putative pheromone receptors in mammals.* Cell, 90, 775-784.

Pin,J.P. and Duvoisin,R. (1995) *The metabotropic glutamate receptors: structure and functions.* Neuropharmacology, 34, 1-26.

Rodriguez,I. (2003) *Nosing into pheromone detectors.* Nat. Neurosci., 6, 438-440.

Rodriguez,I., Feinstein,P. and Mombaerts,P. (1999) *Variable patterns of axonal projections of sensory neurons in the mouse vomeronasal system.* Cell, 97, 199-208.

Rodriguez,I. and Mombaerts,P. (2002) *Novel human vomeronasal receptor-like genes reveal species-specific families.* Curr. Biol., 12, R409-R411.

Runnenburger,K., Breer,H. and Boekhoff,I. (2002) *Selective G protein beta gamma-subunit compositions mediate phospholipase C activation in the vomeronasal organ.* Eur. J. Cell Biol., 81, 539-547.

Ryba,N.J. and Tirindelli,R. (1997) *A new multigene family of putative pheromone receptors.* Neuron, 19, 371-379.

Schild,D. (1989) *Whole-cell currents in olfactory receptor cells of Xenopus laevis.* Exp. Brain Res., 78, 223-232.

Schild,D. and Restrepo,D. (1998) *Transduction mechanisms in vertebrate olfactory receptor cells.* Physiol Rev., 78, 429-466.

Stowers,L., Holy,T.E., Meister,M., Dulac,C. and Koentges,G. (2002) *Loss of sex discrimination and male-male aggression in mice deficient for TRP2*. Science, 295, 1493-1500.

Taniguchi,M., Kashiwayanagi,M. and Kurihara,K. (1996) *Intracellular dialysis of cyclic nucleotides induces inward currents in turtle vomeronasal receptor neurons*. J. Neurosci., 16, 1239-1246.

Taniguchi,M., Wang,D. and Halpern,M. (2000) *Chemosensitive conductance and inositol 1,4,5-trisphosphate-induced conductance in snake vomeronasal receptor neurons*. Chem. Senses, 25, 67-76.

Tirindelli,R., Mucignat-Caretta,C. and Ryba,N.J. (1998) *Molecular aspects of pheromonal communication via the vomeronasal organ of mammals*. Trends Neurosci., 21, 482-486.

Trotier,D. and Doving,K.B. (1996) *Direct influence of the sodium pump on the membrane potential of vomeronasal chemoreceptor neurones in frog*. J. Physiol, 490 (Pt 3), 611-621.

Trotier,D., Doving,K.B., Ore,K. and Shalchian-Tabrizi,C. (1998) *Scanning electron microscopy and gramicidin patch clamp recordings of microvillous receptor neurons dissociated from the rat vomeronasal organ*. Chem. Senses, 23, 49-57.

Vaccarezza,O.L., Sepich,L.N. and Tramezzani,J.H. (1981) *The vomeronasal organ of the rat*. J. Anat., 132, 167-185.

Vogalis,F., Hegg,C.C. and Lucero,M.T. (2005) *Ionic conductances in sustentacular cells of the mouse olfactory epithelium*. J. Physiol, 562, 785-799.

Weiler,E., McCulloch,M.A. and Farbman,A.I. (1999) *Proliferation in the vomeronasal organ of the rat during postnatal development*. Eur. J. Neurosci., 11, 700-711.

Wysocki,C.J. and Lepri,J.J. (1991) *Consequences of removing the vomeronasal organ*. J. Steroid Biochem. Mol. Biol., 39, 661-669.

Zhang,X., Rodriguez,I., Mombaerts,P. and Firestein,S. (2004) *Odorant and vomeronasal receptor genes in two mouse genome assemblies*. Genomics, 83, 802-811.